Modelling of manganese ferroalloy slag properties and flow during tapping

Jacques MULLER[1], Johan H. ZIETSMAN[1], and P. Chris PISTORIUS[2]

1.) University of Pretoria, Pretoria, South Africa

2.) Carnegie Mellon University, Pittsburgh, PA, USA

ABSTRACT

Stable operation of submerged-arc furnaces producing high-carbon ferromanganese (HCFeMn) and silicomanganese (SiMn) requires tapping of consistent amounts of liquid slag and metal. Minimal effort to initiate and sustain tapping at reasonable rates is desired, accommodating fluctuations in especially slag chemical composition and temperature. An analytical model is presented that estimates the tapping rate of the liquid slag-metal mixture as a function of taphole dimensions, coke bed particulate properties, and slag and metal physicochemical properties with dependencies on chemical composition and temperature. This model may be used to evaluate the sensitivity to fluctuations in these parameters, and to determine the influence of converting between HCFeMn and SiMn production.

The model was applied to typical HCFeMn and SiMn process conditions, using modelled slag viscosities and densities. Tapping flow rates estimated were comparable to operational data and found to be dependent mostly on slag viscosity. Slag viscosities were generally lower for typical SiMn slags due to the higher temperature used for calculating viscosity. It was predicted that flow through the taphole would mostly develop into laminar flow, with the pressure drop predominantly over the coke bed. Flow rates were found to be more dependent on the taphole diameter than on the taphole length.

KEY WORDS: *taphole, high-carbon ferromanganese, silicomanganese, physicochemical properties*

1. INTRODUCTION

1.1 Background

Furnace tapping is a key aspect in stable operation of submerged-arc furnaces (SAFs) producing high-carbon ferromanganese (HCFeMn) and silicomanganese (SiMn). These manganese ferroalloys are mostly produced in SAFs through carbothermic reduction of manganese-oxide-bearing ores using carbonaceous reductants (typically coke) and fluxes, with silica also being added to produce SiMn. The stable operation of SAFs requires that consistent amounts of liquid slag and alloy are tapped, and reasonable flow rates should be initiated and sustained with minimal effort in order to maximize the operational efficiency and refractory life. Operational problems can be experienced during tapping, such as difficulties during taphole opening and sluggish or intermittent slag flow. Tapping difficulties are typically compensated for by increasing the operating temperature, changing slag composition, or lancing to open tapholes. These practices cause increased refractory damage over time, as well as other adverse effects on the process and equipment. The operation has to be able to tolerate fluctuations in especially slag chemical composition and temperature. Process differences also have to be accommodated when furnaces are converted between the production of HCFeMn and SiMn with minimal changes to the equipment. The behaviour of slag and alloy in the taphole region and in contact with associated refractory sub-systems is related to physicochemical properties, which are determined by the temperature and chemical composition of the slag and alloy. Slag properties such as viscosity, thermal conductivity, density and surface tension are important process variables that also influence operational aspects such as reaction kinetics, slag-alloy separability, and overall process operability.

Slag chemical compositions and temperatures differ notably between the HCFeMn and SiMn processes and the production practice followed. In the discard slag practice, HCFeMn alloy is produced from ores, reductants, and basic fluxes (CaO, MgO). The product

slag contains low MnO contents of 15 to 20% MnO that is discarded onto slag dumps. In South Africa HCFeMn is mostly produced by smelting ores and reductants in SAFs following the discard slag practice. In countries other than South Africa, the high-MnO slag practice is followed. Slag with 30 to 50% MnO is produced in the HCFeMn process, which is used as primary feedstock together with ores, reductants, quartz, and other fluxes to produce SiMn, also in SAFs. The final slag from the SiMn production contains only around 5% MnO. Process temperatures of the process of interest are notable different with slag tapped from SiMn processes typically ranging between 1823 K to 1923 K (1550 °C to 1650 °C), and between 1673 K to 1773 K (1400 °C and 1500 °C) for HCFeMn processes[1].

A simplified analytical model is presented of flow through a furnace coke bed and taphole in which the tapping flow rate of the liquid slag-metal mixture is calculated as a function of the most important variables: taphole dimensions, coke bed properties, and slag and metal physicochemical properties (derived from its temperature and chemical composition). The typical slags produced in selected HCFeMn and SiMn processes are described by the CaO-MnO-SiO$_2$-Al$_2$O$_3$-MgO system, which comprises the major components found in these slags. The model may be used to evaluate the sensitivity of existing processes to fluctuations in these parameters, and to determine the influence of converting between HCFeMn and SiMn production.

1.2 Previous work

Literature on the modelling of tapping from HCFeMn and SiMn SAFs is scarce, although several studies are reported for iron-producing blast furnaces. The previous work have been reviewed in terms of the modelling methods utilised and the most important conclusions made as basis to formulate a model applicable to the tapping of SAFs.

Physical models of iron-producing blast furnaces have been reported[2,3,4], used in model validations. The 2D and 3D computational fluid dynamics (CFD) approach to model tapping from iron-producing blast furnaces have been reported[2,4,5], which utilised the volume of fluid (VOF) method to represent the gas-liquid or slag-metal interfaces during tapping. Tapping from silicon and ferrosilicon-producing SAFs have been reported by Kadkhodabeigi et al.[6], using also the 2D CFD and VOF approaches. The studies utilising CFD and physical modelling methodologies predominantly focussed on evaluating the effects of internal pressure, coke bed conditions, and taphole conditions on tapping rate and residual amounts of fluid (slag or metal) remaining at the end of tapping, allowing for the consideration of the gas-fluid or slag-metal interface shape.

Out of the iron-producing blast furnace CFD studies reported, Nishioka et al.[2] concluded the taphole diameter to be dominant in determining the total tapping rate, with the permeability of the coke bed affecting the residual fluid levels after tapping. However, Iida et al.[7] subsequently reported on an analytical tapping model of an iron-producing blast furnace, concluding the effect of the hearth temperature to be significant on the coke bed permeability and on tapping rates. The model by Iida et al.[7] required the coke bed fluid path length to be specified, and assumed the linear fluid flow rate to be the same through the coke bed and taphole, which negatively affected the reliability of the modelled results if not validated against plant data. Therefore, to develop a representative tapping model of the SAF process (with a significantly lower internal pressure) it is necessary to include modelling of fluid flow through both the taphole and coke bed pressure. Improved modelling of the taphole friction factors and the tapped mixed-fluid physicochemical properties are also needed, as well as improvement in the methodology to model the coke bed pressure drop to eliminate uncertainties.

2. MODELS

2.1 Slag properties

As input to a tapping flow model, the viscosity and density of typical slags produced in HCFeMn and SiMn processes are required. Such physicochemical properties are dependent on the slag structure (determined by its chemical composition) and temperature[8]. The effect that different process conditions have on tapping was incorporated into this study by modelling viscosity and density as functions of chemical composition and temperature. In this study values were derived for typical slag compositions and at typical operating temperatures for use in the tapping flow model.

FactSage[9] was firstly used to calculate the phase equilibrium for a given slag chemical composition and a temperature. From the phase equilibrium results the amounts of solids and liquids were derived and used in slag viscosity and density calculations. Slag liquid viscosity was estimated using a model from Mills *et al.*[8], based on the Urbain formalism in which viscosity is related to temperature with the Weymann relationship.

To calculate viscosity, the mole fractions of slag constituents are firstly grouped into glass formers (SiO_2), modifiers (CaO, MgO, MnO), and amphoterics (Al_2O_3).

$$X_G = X_{SiO_2} \tag{1}$$

$$X_M = X_{CaO} + X_{MgO} + X_{MnO} \tag{2}$$

$$X_A = X_{Al_2O_3} \tag{3}$$

The α-ratio is calculated as:

$$\alpha = \frac{X_M}{(X_M + X_A)} \tag{4}$$

The B-parameter for the Urbain-viscosity model is calculated as:

$$B = B_0 + B_1 X_G + B_2 X_G^2 + B_3 X_G^3 \tag{5}$$

The individual B-parameters are calculated as:

$$B_0 = 13.8 + 39.9355\,\alpha - 44.049\,\alpha^2 \tag{6}$$

$$B_1 = 30.481 - 117.1505\,\alpha + 139.9978\,\alpha^2 \tag{7}$$

$$B_2 = -40.9429 + 234.0486\,\alpha - 300.04\,\alpha^2 \tag{8}$$

$$B_3 = 60.7619 - 153.9276\,\alpha + 211.1616\,\alpha^2 \tag{9}$$

The A-parameter is calculated:

$$-\ln A = 0.2693\,B + 11.6725 \tag{10}$$

The liquid slag viscosity can then be calculated:

$$\mu_{liquid} = A\,T\exp(10^3 B\,/\,T) \tag{11}$$

The volume fraction of solids, estimated with FactSage, was used with the Roscoe equation[11] to adjust the liquid viscosity and yield the effective viscosity:

$$\mu_{effective} = \mu_{liquid}(1 - 1.35\,\varphi_{solids})^{-2.5} \tag{12}$$

The density of solid and liquid slags were modelled individually as functions of composition and temperature, and then combined to obtain the density of the multiphase mixtures. The molar volume of solid slag at 298 K can be calculated using the partial molar volumes of the components[10]:

$$\bar{V}_{298\,K} = \left(23.76 + 3.5X_{SiO_2}\right)X_{SiO_2} + 40.4\,X_{Al_2O_3} + 14.4X_{CaO} + 12.5X_{MgO} + 17\,X_{MnO} \tag{13}$$

The density of solid slag can then be calculated using a thermal expansion coefficient[10]:

$$\rho_{solid} = \rho_{298K}/(1 + 9 \times 10^{-6}\,\Delta T)^3 \tag{14}$$

The density of the liquid slag at 1673 K was calculated using the following relationship as a function of the mass fraction of MnO only[12], and a thermal expansion coefficient of 1 x 10^{-4} K^{-1}:

$$\rho_{1673\,K} = 2490 + 12\,w_{MnO} \qquad [15]$$

The density of the multiphase slag mixture can then be calculated:

$$\rho_{slag\ mixture} = (1 - \varphi_{solids})\rho_{solid} + \varphi_{solids}\,\rho_{liquid} \qquad [16]$$

2.2 Liquid slag-metal mixture properties

The fluid for which flow is modelled is a mixture of slag and metal, allowing for the fraction of each to vary as it would throughout the progression of the tap. The density and viscosity of a liquid slag-metal mixture are typically estimated simply as the mean of the respective values[7], irrespective of varying relative amounts of each material.

The viscosity and density of the liquid slag-metal mixture were both estimated using the rule of mixtures approach as the weighted averages of viscosity and density of slag and metal respectively for varying volume fractions of each liquid.

The average liquid mixture density is calculated by Equation [17]:

$$\rho_{mixture} = \varphi_{slag}\rho_{slag} + \varphi_{metal}\rho_{metal} \qquad [17]$$

The average liquid mixture viscosity is calculated by Equation [18]:

$$\mu_{mixture} = \varphi_{slag}\mu_{slag} + \varphi_{metal}\,\mu_{metal} \qquad [18]$$

In addition to the rule of mixtures, the use of a model from Pal[13] was evaluated, which considers the liquid slag-metal mixture as a concentrated emulsion, with viscosity a function of the continuous and dispersed phases and the volume fraction of the dispersed phase. This model assumes the two fluids to be sufficiently finely dispersed in one another. The effective viscosity of the liquid slag-metal mixture is modelled with the following equations [13]:

$$\mu_r \left[\frac{2\mu_r + 5K}{2 + 5K}\right]^{3/2} = \left(1 - \frac{\varphi_{dispersed}}{\varphi_m}\right)^{-2.5\varphi_m} \qquad [19]$$

$$\mu_{mixture} = \mu_r \times \mu_{continuous} \qquad [20]$$

2.3 Analytical tapping flow model

Spherical-radial flow through the coke bed:

The model is based on the iron blast furnace tapping flow modelling work reported by Iida *et al.*[7], with flow rate solved from equations of pressure drop across the coke bed and taphole. In the simplified model domain (Fig. 1) the coke bed is represented by a hemispherical volume around the taphole entry region with the fluid flow paths along the radius of the hemisphere. This domain configuration assumes a constant inlet pressure for all flows with the spherical pressure drop variation to be dominant over the variation with height, and also implicitly ignores other possible flow mechanisms around the taphole inlet area. This domain is different from the linear fluid flow path through a coke bed of specified length used in the model reported by Iida *et al.*[7], and allows for the equation for pressure drop across the coke bed to become independent of the length of the fluid path through the coke bed.
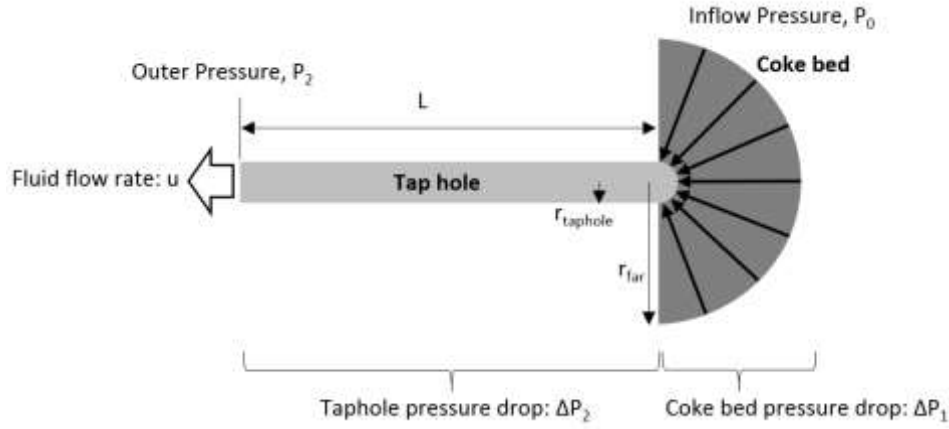
Fig. 1 The model domain, with fluid flow through the taphole and spherical-radial flow through the coke bed.

The pressure drop across the coke bed is found by integration of the Kozeny-Carman equation [7] from the taphole radius to some point remote from the taphole:

$$\Delta P_1 = \int_{r_{taphole}}^{r_{far}} \frac{90\, V\, \mu}{\pi\, r^2\, D^2} \cdot \frac{(1-\varepsilon)^2}{\varepsilon^3} \cdot dr = \frac{90 V \mu}{\pi D^2} \cdot \frac{(1-\varepsilon)^2}{\varepsilon^3} \cdot \left(\frac{1}{r_{taphole}} - \frac{1}{r_{far}} \right) \tag{21}$$

The length of coke bed through which fluid flows is expected to be significantly larger than the radius of the taphole, i.e. $r_{far} \gg r_{taphole}$. In Equation [5] the maximum pressure drop is calculated for an infinitely large hemisphere, where r_{far} is set equal to infinity, and Equation [5] can then be simplified to yield Equation [22] that is independent of the unknown thickness of the coke bed fluid path. It can be shown from Equation [5] that 50% of the maximum pressure drop will occur within the distance of only one taphole diameter and 75% of the maximum pressure drop within two taphole diameters, indicating that the large value of r_{far} required for this simplification is assumed to be within typical thickness of coke bed.

$$\Delta P_1 = \frac{90 V \mu}{\pi D^2} \cdot \frac{(1-\varepsilon)^2}{\varepsilon^3} \cdot \frac{1}{r_{taphole}} \tag{22}$$

The coke bed void fraction and particle diameter parameters are expected to be related, and it is possible to further simplify Equation [22] by combining these parameters into a single parameter indicating the bed permeability.

Flow through the taphole:

The flow regime through the taphole is related to the fluid properties and the average velocity by calculating the Reynolds number, with values typically up to 2100 indicating laminar flow, whereafter flow is indicated to be turbulent[14]. The Reynolds number is calculated here considering the taphole to be a circular duct [14]:

$$Re = \frac{\rho d u}{\mu} \tag{23}$$

Equation [23] for the Reynolds number differs from that reported by Iida et al.[7] in that the taphole diameter, d, is used here instead of the taphole length. The Darcy-Weisbach equation [14] is used to model flow through a cylindrical tube, considering the fluid flowing through the coke bed, entering the taphole at the one end and exiting at the other end. The pressure drop, ΔP_2, is estimated as follows:

$$\Delta P_2 = f \frac{L}{d} \cdot \frac{\rho u^2}{2} \tag{24}$$

The friction factor in Equation [24] can be calculated specifically for either fully developed laminar flow or for turbulent flow by using experimentally determined correlations. For the tapholes considered with typically low length-to-diameter ratios, flow is expected not to develop into fully laminar flow. In such cases, where flow is in the transitional entry region of a tube, the Darcy-Weisbach friction factor can be up to four times larger than that of fully developed laminar flow[15]. The apparent friction factor for developing laminar flow (Re < 2100), f_{app}, is calculated using the correlation by Ghajar and Madon[15]:

$$f_{app} = \frac{1}{Re}\left(\frac{3.44}{\zeta^{1/2}} + \frac{0.31/\zeta + 16 - 3.44/\zeta^{1/2}}{1 + 0.00021/\zeta^2}\right) \qquad [25]$$

$$\zeta = \frac{L}{d\,Re} \qquad [26]$$

The apparent friction factor for turbulent flow (Re > 2100), $f_{turbulent}$, is calculated using the empirical Haaland equation[16]:

$$f_{turbulent} = \frac{4}{\left(3.6\log\left(\frac{Re}{6.9}\right)\right)^2} \qquad [27]$$

2.4 Furnace operating conditions

Typical slags produced in HCFeMn and SiMn processes were identified and used in the application of the models to evaluate the tapping flow. The slag compositions (Table I) were selected to cover a wide operating range of slag compositions from the most common practices. These include typical compositions obtained from literature and from a South African HCFeMn producer.

Table I

Typical HCFeMn and SiMn slag compositions used in taphole flow modelling.

Specie	Slag compositions (wt.%)						
	HCFeMn A[1]	HCFeMn B[1]	HCFeMn C[2]	HCFeMn D[2]	SiMn A[1]	SiMn B[3]	SiMn C[3]
	Duplex process	Discard practice	Discard practice	Discard practice			
MnO	40.9	15.1	29.8	36.0	8.5	7.7	3.1
SiO$_2$	23.1	24.0	30.0	24.0	45.2	42.1	41.8
Al$_2$O$_3$	12.7	20.7	4.3	16.0	15.8	20.9	20.0
CaO	16.9	34.4	29.3	20.0	21.0	22.4	29.0
MgO	6.4	5.7	6.6	4.0	9.5	6.9	6.2
Basicity*	1.79	1.23	1.91	1.5	0.64	0.59	0.62

1. Olsen et al.[1]; 2. Typical from a South African HCFeMn producer; 3. Mølnås[17].

* Basicity = (CaO+MgO+MnO)/(Al$_2$O$_3$+SiO$_2$)

To evaluate the reliability of the tapping flow model the results are compared against typical tapping rates inferred from data in literature. Both HCFeMn and SiMn furnaces are tapped intermittently at regular intervals of typically 2 to 3 hours, with taps lasting for 20 to 40 minutes[17]. Typical amounts of alloy tapped are 30 to 50 tons of HCFeMn, and 10 to 30 tons of SiMn[1]. Average slag and alloy tapping rates are estimated for HCFeMn and SiMn furnaces and presented in Table II with relevant operational data from Olsen et al.[1]. Tapping rates were calculated from the slag and alloy production data, assuming tapping every 2 hours through a taphole with a diameter of 100 mm, and a tap duration of 20 minutes.

Table II

Slag and alloy tapping results derived from typical industrial data[1].

Parameter	Units	HCFeMn, high-MnO slag		SiMn
Furnace power	MW	30	33.3	27
Alloy production	t.d^{-1}	294	395.5	175
Slag rate	kg slag.t^{-1} alloy	640	640	1225
Alloy produced in 2 hours	t alloy	24.5	33.0	14.6
Slag produced in 2 hours	t slag	15.7	21.1	17.9
Alloy density	kg.m^{-3}	5612	5612	4449
Slag density	kg.m^{-3}	3300	3300	2700
Alloy tapping mass flow rate	kg.s^{-1}	20.4	27.5	12.2
Slag tapping mass flow rate	kg.s^{-1}	13.1	17.6	14.9
Total tapping mass flow rate	kg.s^{-1}	33.5	45.0	27.0
Alloy volumetric tapping rate	m^3.s^{-1}	0.0036	0.0049	0.0027
Slag volumetric tapping rate	m^3.s^{-1}	0.0040	0.0053	0.0055
Total volumetric tapping rate	m^3.s^{-1}	0.0076	0.0102	0.0082
Average volume fraction slag		0.52	0.52	0.67
Alloy velocity	m.s^{-1}	0.463	0.623	0.348
Slag velocity	m.s^{-1}	0.504	0.678	0.702
Total fluid velocity	m.s^{-1}	0.967	1.301	1.050

The results from the comprehensive CFD model of a FeMn furnace reported by Kadkhodabeigi[18] are also considered. The model reported by Kadkhodabeigi[18] assumed a slag production rate of 200 t.d^{-1}, and an alloy rate of 330 t.d^{-1} as source terms. For assumed slag and alloy heights each 0.5 m above the taphole, the total tapping rate was estimate to decrease from approximately 47 kg.s^{-1} at the start of the tap, to below 20 kg.s^{-1} by the end of the tap. At the start of the tap, the total flow estimated consisted of mostly alloy that decreased over the duration of the tap, with the slag rate increasing to a maximum of approximately 18 kg.s^{-1} around 17 minutes into the tap.

2.5 Tapping flow model parameters

The tapping flow model was firstly applied to the iron blast furnace using the model parameter values reported by Iida et al.[7]. These parameter values are summarised in Table III, and exclude the length of the coke bed fluid path, since the model reported here is independent of this parameter (Equation [22]). The volume fraction of slag has been varied between 0.5 and 1 in this study, whereas Iida et al.[7] reports for a slag fraction of 0.5 only.

Table III

Iron blast furnace[7] and HCFeMn and SiMn SAF tapping flow model parameter values.

Parameter	Symbol	Units	Iron blast furnace[7]	HCFeMn and SiMn SAF
Coke particle diameter	D	m	0.04	0.05
Coke filter void fraction	ε		0.32	0.3
Slag density	ρ_{slag}	kg.m^{-3}	2800	2476 – 2992

Parameter	Symbol	Units	Iron blast furnace[7]	HCFeMn and SiMn SAF
Metal density	ρ_{metal}	kg.m^{-3}	6700	SiMn: 4449; HCFeMn: 5612
Slag viscosity	μ_{slag}	Pa.s	0.435	0.64 – 1.54
Metal viscosity	μ_{metal}	Pa.s	0.006	0.005
Slag ratio (vol. fraction slag)	SR	Vol. fraction	0.5 – 1	0.5 – 1
Total pressure drop	$P_2 - P_0$	Pa	300 000	15 000 – 29 318
Taphole length	L	m	3.5	0.6
Taphole diameter	d	m	0.06	0.1
Slag Height	h_{slag}	m		0.0; 0.5
Metal Height	h_{metal}	M		0.0

The tapping flow model was applied to evaluate tapping from SAFs producing SiMn and HCFeMn. For this application a specific set of values were defined for the model parameters representing the domain geometry, slag and metal physicochemical properties, coke bed particulate properties, and boundary conditions. The model parameter values, summarised in the last column of Table III, have been selected as follows:

- *Domain geometry*: A taphole length of 0.6 m and taphole diameter of 0.1 m were used. Initial slag heights of 0 and 0.5 m were investigated to establish the range of flow rates estimated as slag is being tapped, and the metal height set at 0 m, i.e. at the level of the taphole[18].

- *Slag physicochemical properties*: Densities and viscosities of the typical SiMn and HCFeMn slags were modelled for a tap temperature of 1673 K (1400 °C) for HCFeMn slags and 1873 K (1600 °C) for SiMn slags[1].

- *Metal physicochemical properties*: A viscosity of 0.005 Pa.s was used by Kadkhodabeigi[18] and applied here for both SiMn and HCFeMn alloys. SiMn and HCFeMn alloy densities were calculated using the models of Crawley[19], Jimbo and Cramb[20], and Nasch and Steinemann[21]. Averages were used of alloy chemical compositions provided by Olsen et al.[1].

- *Coke bed particulate properties*: A coke bed particle diameter of 0.05 m and void fraction of 0.3 were used for the coarse coke bed by Kadkhodabeigi[18] in the 2D CFD modelling of the FeMn SAF tapping process.

- *Inlet pressure*: The total pressure drop is specified as the difference between the inlet pressure (P_0) and the taphole outlet pressure (P_2). The total pressure drop was calculated as 15 000 Pa to account for the weight of the burden on the slag[18], and adding the hydrostatic pressure calculated for a slag height of 0.5 m and using the modelled density of each slag.

3. RESULTS AND DISCUSSION

3.1 Slag viscosity and density

Viscosities and densities of the typical HCFeMn and SiMn slag compositions were calculated (Table I) at a standard operating temperature of 1673 K (1400 °C) for HCFeMn slags and 1873 K (1600 °C) for SiMn slags. The viscosity and density calculations considered the percentage solids derived from the equilibrium phase composition determined with FactSage[9]. Fig. 2 shows the liquidus temperature pseudo-ternary diagram with the typical slag compositions plotted to indicate the solid phases that could be expected at the typical slag temperatures.
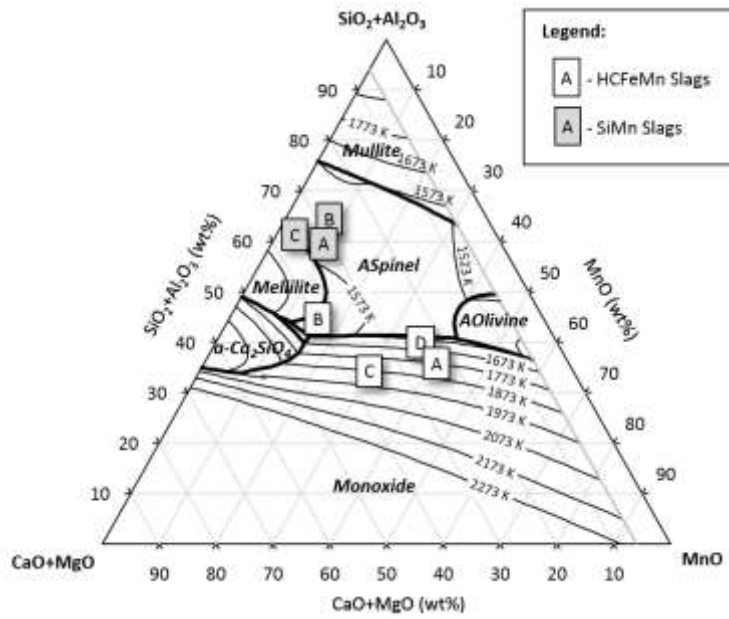
Fig. 2 Liquidus temperature pseudo-ternary diagram of the CaO-MnO-SiO$_2$-Al$_2$O$_3$-MgO slag system with 6% MgO and Al$_2$O$_3$/SiO$_2$= 0.57, showing typical SiMn and HCFeMn slag compositions (Table I), calculated with FactSage[9].

The modelled slag viscosities and densities are listed with the tapping flow model results in Table VI and Table VII. Results indicate both viscosity and density to be generally higher for the HCFeMn slags as compared to the SiMn slags, with the exception the viscosity of slag HCFeMn C being lower than the viscosities of all the SiMn slags. Estimated effective slag viscosities (Fig. 3 and Fig. 4) and densities (Fig. 5 and Fig. 6) are illustrated as functions of basicity and temperature, calculated using as baselines the typical HCFeMn and SiMn slag compositions (Table I), and standard operating temperatures. The curves for slags SiMn B and C were omitted for being similar to that of slag SiMn A, and that of HCFeMn D was also excluded for being similar to that of slag HCFeMn A. These results indicate notable differences in the baseline viscosities and densities due to the significant differences in chemical composition and operating temperatures of the typical SiMn and HCFeMn slag compositions (Table I).

Fig. 3 illustrates that an increase in basicity would cause decreasing viscosities of typical SiMn slags due to the effect of network-breaking monoxides, while viscosity tends to increase with increased basicity for HCFeMn slags as monoxide phase solids precipitate at higher basicities. When operating above the liquidus temperature, viscosity will increase with increased SiO$_2$ content as the longer polymer chains cause resistance to flow, while below the liquidus temperature higher SiO$_2$ contents lead to fewer flow-hindering precipitated solids and decreasing viscosity. The effect of precipitation is also seen in Fig. 4, where the effective viscosity increases with cooling from higher temperatures, with an abrupt increase from the liquidus temperature as solids start to precipitate.
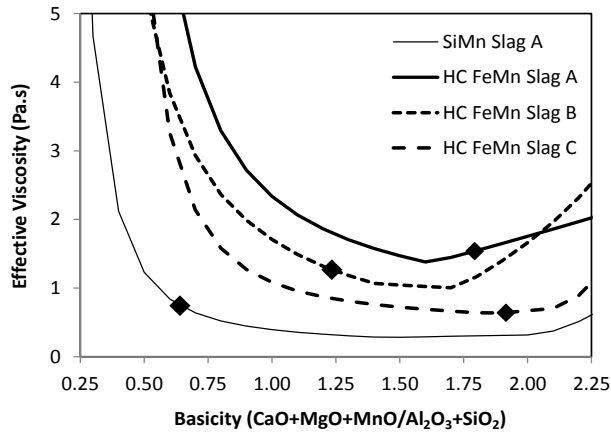
Fig. 3 Effective slag viscosity as a function of basicity (CaO+MgO+MnO/SiO$_2$+Al$_2$O$_3$) around that of the baseline compositions, and at 1673 K (1400 °C) for HCFeMn slags and at 1873 K (1600 °C) for SiMn slags. Solid markers indicating values calculated at the baseline slag compositions selected.
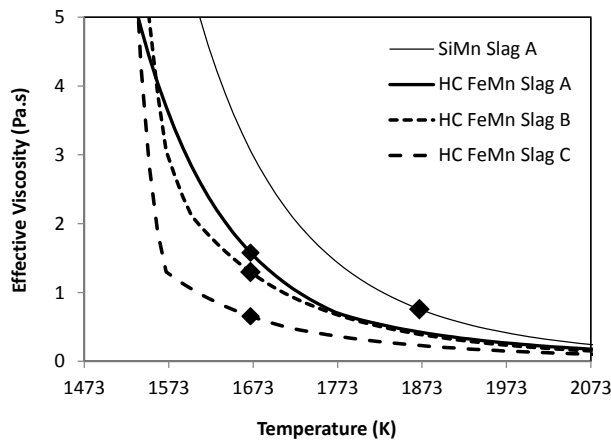

Fig. 4 Effective slag viscosity as a functions of temperature for the baseline compositions. Solid markers indicating values calculated at 1673 K (1400 °C) for HCFeMn slags and at 1873 K (1600 °C) for SiMn slags.

Densities are estimated to increase with basicity (Fig. 5) as a result of the lower molar volumes and higher densities of constituents with higher basicities (basic oxides). Over the basicity range, densities of typical SiMn slags are estimated to be lower than typical HCFeMn slags, due largely to the higher SiO$_2$ contents with high molar volumes and lower MnO contents of SiMn slags, as well as the difference in baseline temperatures for which the results were calculated (1673 K (1400 °C) for HCFeMn slags and 1873 K (1600 °C) for SiMn slags). Density is estimated to decrease with temperature (Fig. 6) due to thermal expansion, and due to the liquids having lower densities than solids. Above the liquidus temperature, density would decrease more rapidly, since with liquid slag has a larger thermal expansion coefficient.
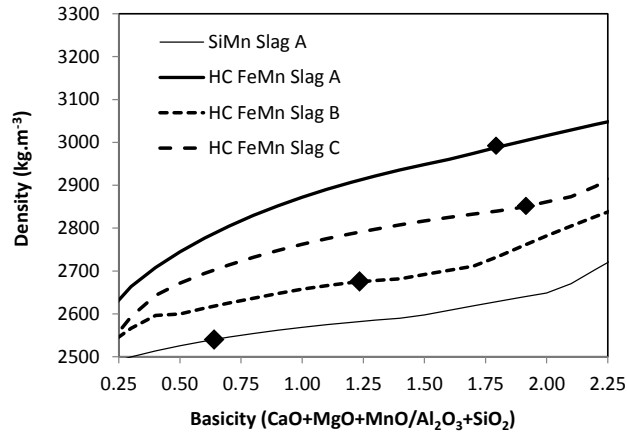
Fig. 5 Slag density as a function of basicity ($CaO+MgO+MnO/SiO_2+Al_2O_3$) around that of the baseline compositions, and at 1673 K (1400 °C) for HCFeMn slags and at 1873 K (1600 °C) for SiMn slags. Solid markers indicating values calculated at the baseline slag compositions selected.
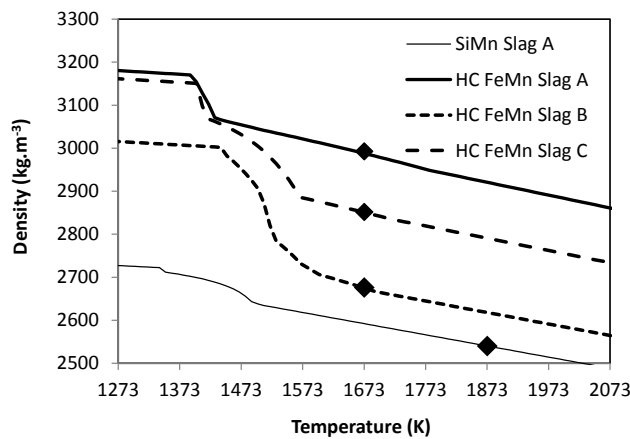

Fig. 6 Slag density as a functions of temperature for the baseline compositions. Solid markers indicating values calculated at 1673 K (1400 °C) for HCFeMn slags and at 1873 K (1600 °C) for SiMn slags.

3.2 Liquid slag-metal mixture viscosity

The calculation of the liquid slag-metal mixture viscosity is evaluated where the fluid is considered to be a concentrated emulsion using the model from Pal[13], as described by Equation [19] and [20]. The influence of the selection of dispersed and continuous phases is illustrated in Fig. 7, calculated using a slag viscosity of 0.435 Pa.s and a metal viscosity of 0.006 Pa.s[7]. The diagram shows the estimated liquid mixture viscosity as a function of the volume fraction of slag, where either slag (curve 1) or metal (curve 2) was selected as the dispersed phase. In either case the volume fraction of the dispersed phase, φ, is constrained to 0.637 (the value of the model fitting parameter, φ_m) due to the formulation of Equation [19]. For slag fractions between 0.363 and 0.637 it is therefore possible to select either slag or metal as the dispersed phase. For this slag fraction range the liquid mixture viscosity is estimated to be within the range of viscosities defined by the two curves in Fig. 7.

11

For the selection of metal as the dispersed phase (curve 2), the estimated viscosities increase significantly below slag fractions of around 0.5. This is not considered to be realistic – for example, a mixture with 40% metal is not expected to have a viscosity so high that almost no flow would occur. Considering the viscosity ratios of the emulsion systems used from Pal[13], the derived model would in most cases also be expected to be valid only up to dispersed phase fractions, φ, of around 0.5. At this point a large discontinuity exists in the estimated viscosities, as can be seen from the difference between the curves at a slag fraction of 0.5 (Fig. 7).

This mixture model from Pal[13] was further evaluated in the tapping flow model, considering only the scenario with metal as the dispersed phase and slag as the continuous phase, with slag fractions from 0.5 to 1.
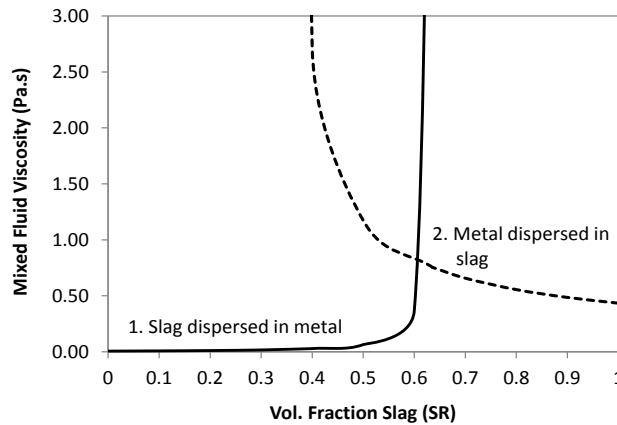

Fig. 7 Estimated liquid mixture viscosity as a function of the volumetric slag fraction using the model from Pal[13], alternating selected dispersed and continuous phases.

3.3 Iron blast furnace application

As part of the evaluation of the tapping flow model presented here, the model was applied for the iron blast furnace using the same parameter values used by Iida et al.[7] (Table III), and varying the fraction of slag tapped. Results are compared to that obtained by Iida et al.[7] where flow rates were estimated to decrease from approximately 0.036 to 0.014 $m^3.s^{-1}$ for coke bed fluid path lengths increasing from 0.01 to 0.15 m, and a rate of 0.021 $m^3.s^{-1}$ was obtained for a baseline coke bed fluid path length of 0.08 m.

Table IV

Iron blast furnace tapping flow model results, calculating the liquid mixture viscosity using the model from Pal[13] with metal as dispersed phase.

			Slag ratio, SR:			
Parameter	Symbol	Units	0.5	0.6	0.6	1
Flow regime used for friction factor			Laminar	Laminar	Turbulent	Turbulent
Liquid mixture density	ρ_{avg}	kg.m^{-3}	4750	4360	4360	2800
Liquid mixture viscosity	μ_{avg}	Pa.s	1.17	0.82	0.82	0.44
Reynolds nr.	Re		1746	3028	1692	3007
Friction factor	f		0.014	0.010	0.054	0.044
Coke bed pressure drop	ΔP_1	Pa	200 643	187 356	104 651	80 650

			Slag ratio, SR:			
Parameter	**Symbol**	**Units**	**0.5**	**0.6**	**0.6**	**1**
Taphole pressure drop	ΔP_2	Pa	99 357	112 644	195 349	219 350
Total pressure drop	ΔP_{tot}	Pa	300 000	300 000	300 000	300 000
Fluid flow velocity	u	m.s⁻¹	7.185	9.544	5.331	7.786
Fluid volumetric rate	V	m³.s⁻¹	0.020	0.027	0.015	0.022
Fluid mass rate	M	kg.s⁻¹	96.5	117.6	65.7	61.6

The tapping model results for the liquid mixture viscosity calculated with the model from Pal[13] are summarised in Table IV and results from using the rule of mixtures to estimate viscosity in Table V. For a slag fraction of 0.5 a total tapping rate of 0.020 m³.s⁻¹ was calculated using the viscosity model from Pal[13], while a total tapping rate of 0.022 m³.s⁻¹ was calculated using the rules of mixtures to estimate the liquid mixture viscosity, corresponding to the observed value of 0.021 m³.s⁻¹. The difference in estimated flow rates are small between the two viscosity models at a slag fraction of 0.5, but significant differences exist in the other result parameters. The significantly higher viscosity from using the model from Pal[13] is balanced by a low friction factor resulting from a change in the flow regime being laminar. When using the model from Pal[13] a high liquid mixture viscosity of 1.17 Pa.s is estimated, resulting in a Reynolds number of 1746 (laminar flow) and a low taphole friction factor of 0.014, and the dominant pressure drop calculated to be over the coke bed (Table IV). A significantly lower liquid mixture viscosity of 0.22 Pa.s is estimated with the rule of mixtures, resulting in a higher Reynolds number of 10 067 (turbulent flow) and a high friction factor of 0.031, with the dominant pressure drop over the taphole (Table V).

Table V

Iron blast furnace tapping flow model results, calculating the liquid mixture viscosity using the rule of mixtures.

			Slag ratio, SR:		
Parameter	**Symbol**	**Units**	**0.5**	**0.6**	**1**
Flow regime used for friction factor			Turbulent	Turbulent	Turbulent
Liquid mixture density	ρ_{avg}	kg.m⁻³	4750	4360	2800
Liquid mixture viscosity	μ_{avg}	Pa.s	0.22	0.26	0.44
Reynolds nr.	Re		10 067	7658	3007
Friction factor	f		0.031	0.033	0.044
Coke bed pressure drop	ΔP_1	Pa	40 896	48 364	80 650
Taphole pressure drop	ΔP_2	Pa	259 104	251 636	219 350
Total pressure drop	ΔP_{tot}	Pa	300 000	300 000	300 000
Fluid flow velocity	u	m.s⁻¹	7.789	7.711	7.786
Fluid volumetric rate	V	m³.s⁻¹	0.022	0.022	0.022
Fluid mass rate	M	kg.s⁻¹	104.6	95.1	61.6

The estimated total volumetric flow rates are illustrated in Fig. 8 and Fig. 9 as functions of the fraction slag tapped. Fig. 8 shows that when using the model from Pal[13] flow rates were estimated to increase with the slag fraction being tapped, as the liquid mixture viscosity was estimated to decrease with less of the dispersed phase (metal) present. For this particular application for slag fractions between 0.527 and 0.683, discontinuities in the estimated flow rates resulted from the differences in the friction factors for laminar and turbulent flow, and hence these are separately illustrated in Fig. 8. Results in Table IV illustrate this discontinuity, by using the laminar friction factor at a slag fraction of 0.6, a high flow rate is estimated and subsequently a Reynolds number larger than 2100 is obtained.

Should the higher turbulent friction factor be used, as indicated by the Reynolds number larger than 2100, a lower flow rate is estimated and the Reynolds number is then again significantly less than 2100, suggesting that the laminar friction factor should be used.

By using the rule of mixtures approach to estimate the liquid mixture viscosity, tapping rates could be estimated for slag fractions from 0 to 1 as illustrated in Fig. 9. Over the full range of slag fractions, turbulent flow was obtained as a result of overall lower mixture viscosities and higher flow rates for lower slag fractions, compared to using the viscosity model from Pal[13]. A volumetric flow rate of 0.032 $m^3.s^{-1}$ was estimated when tapping only metal (SR = 0), decreasing to 0.022 $m^3.s^{-1}$ at a slag fraction of 0.5. For slag fractions of 0.5 to 1 the flow rate was estimated to be almost constant at 0.022 $m^3.s^{-1}$ as the liquid mixture density decreases despite an increasing taphole friction factor due to increasing mixture viscosities and decreasing Reynolds numbers. This agreement with observed tapping rates when using the rule of mixtures to estimate viscosity (Fig. 9), indicate the application of the liquid mixture viscosity from Pal[13] is less likely to be valid for this model input parameter set, and especially so at slag fractions below 0.683.
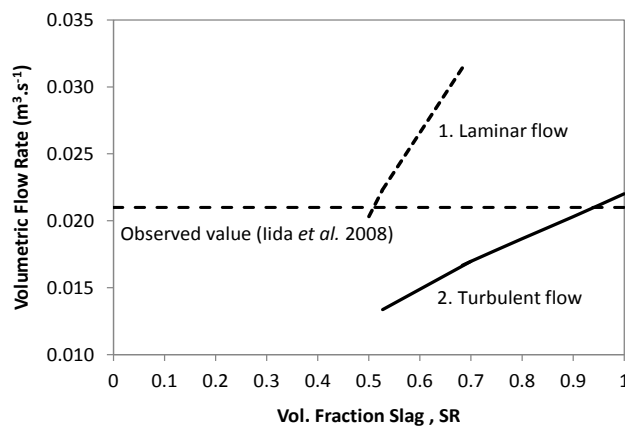

Fig. 8 Total volumetric flow rates estimated for an iron blast furnace as a function of volume fraction slag, with the liquid mixture viscosity calculated using the model from Pal[13] with metal as dispersed phase.
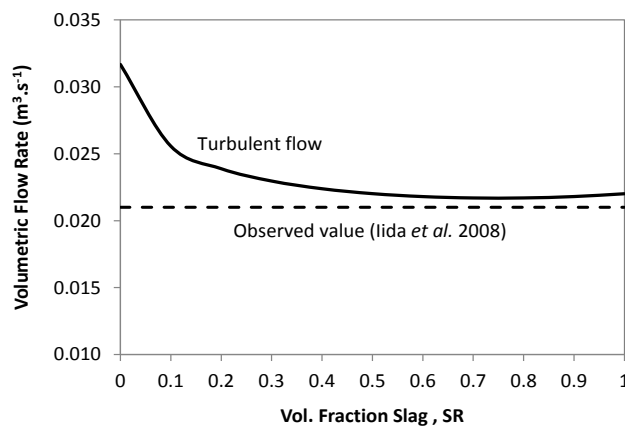

Fig. 9 Total volumetric flow rates estimated for an iron blast furnace as a function of volume fraction slag, with the liquid mixture viscosity calculated using the rule of mixtures.

3.4 HCFeMn and SiMn SAF tapping modelling

The tapping flow model reported was applied to evaluate tapping rates from SiMn and HCFeMn SAFs using the relevant model parameter values in Table III, varying the fraction of slag tapped (0.5 and 1) and the height of slag above the taphole (0 and 0.5 m) to simulate the varying slag-alloy ratio and decreasing slag height throughout tapping. The models used for calculating the liquid mixture viscosity was again evaluated with Fig. 10 showing estimated total tapping flow rates using the model from Pal[13] and Fig. 11 for calculating viscosity with the rule of mixtures, illustrated as functions of the effective slag viscosities. Fig. 10 and Fig. 11 also indicate the range of total volumetric flow rates expected, as calculated from data from Olsen *et al.*[1] (Table II).

The general sensitivity of tapping rate to variations in slag viscosity due to operating practices when using either of the viscosity models is illustrated in Fig. 10 and Fig. 11. With the liquid mixture viscosity model from Pal[13] (Fig. 10), total tapping rates were estimated to be within the range of expected values only at the greater slag height (0.5 m above the taphole) and for higher fractions of slag with lower viscosities (SiMn, HCFeMn C) due to the liquid mixture viscosity modelled to decrease with the decreasing fractions of dispersed alloy[13]. Higher flow rates were estimated using the rule of mixtures to calculate viscosity (Fig. 11) for slag fraction below 1 due to the liquid mixture viscosity decreasing with increasing alloy fractions. Tapping rates are illustrated in Fig. 11 to be below the typical values when tapping slag of higher viscosities, and at lower slag heights similar to what would occur towards the end of tapping. It is therefore concluded, similar to the iron blast furnace application, that the viscosity model by Pal[13] for finely dispersed mixtures is not likely to be valid for HCFeMn and SiMn SAF conditions. The results indicate that separated flow is rather expected, and that the rule of mixtures approach is more accurate, yielding tapping rates closer to expected values.

Fig. 10 Total volumetric flow rate as a function of viscosity for typical SiMn and HCFeMn slags, varying slag heights and slag fractions (SR), with the liquid mixture viscosity calculated using the model from Pal[13] with alloy as dispersed phase.
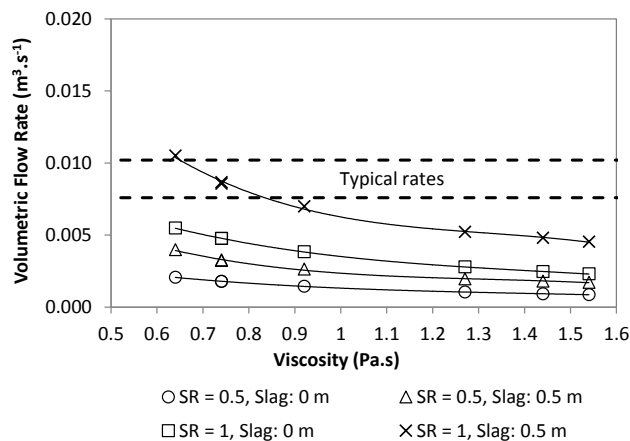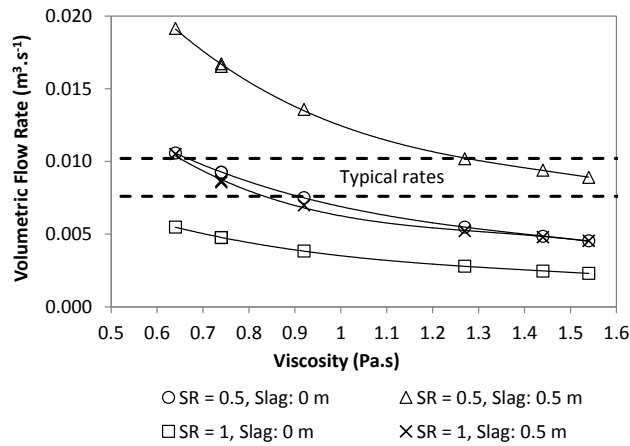
Fig. 11 Total volumetric flow rate as a function of viscosity for typical SiMn and HCFeMn slags, varying slag heights and slag fractions (SR), with the liquid mixture viscosity calculated using the rule of mixtures.

Of the tapping flow model results illustrated in Fig. 10 and Fig. 11, result values are summarised in Table VI for a slag height of 0.5 m above the taphole and a slag fraction of 0.5, using the rule of mixtures to calculate the liquid mixture viscosity. Results are summarised in Table VII for tapping only slag at a height of height of 0.5, therefore independent of the liquid mixture viscosity model. Reynolds numbers calculated were below 2100 and indicated laminar flow (except for HCFeMn C at a slag fraction of 0.5), resulting in lower taphole friction factors and pressure drops to be dominant over the coke bed. As tapping progresses the slag height would decrease, in which case the hydrostatic pressure and flow rate would also decrease, and the flow would therefore remain laminar.

Table VI

SiMn and HCFeMn SAF tapping flow model results for a slag fraction of 0.5 and slag height at 0.5 m above the taphole (effective viscosity with rule of mixtures).

Parameter	Symbol	Units	SiMn process			HCFeMn process			
			SiMn A	SiMn B	SiMn C	HCFeMn A	HCFeMn B	HCFeMn C	HCFeMn D
Slag density	ρ_{slag}	kg.m^{-3}	2540	2531	2476	2992	2676	2852	2922
Slag viscosity	μ_{slag}	Pa.s	0.74	0.92	0.74	1.54	1.27	0.64	1.44
Liquid mixture density	ρ_{avg}	kg.m^{-3}	3495	3490	3463	4302	4144	4232	4267
Liquid mixture viscosity	μ_{avg}	Pa.s	0.37	0.46	0.37	0.77	0.64	0.32	0.72
Reynolds nr.	Re		1997	1304	1957	632	843	3200	707
Friction factor	f		0.033	0.041	0.033	0.062	0.053	0.043	0.058
Coke bed pressure drop	ΔP_1	Pa	25 900	26 114	25 617	28 629	27 009	25 695	28 248
Taphole pressure drop	ΔP_2	Pa	1548	1288	1517	1034	1102	3279	1069
Total pressure drop	ΔP_{tot}	Pa	27 448	27 403	27 133	29 663	28 111	28 973	29 318
Fluid flow velocity	u	m.s^{-1}	2.128	1.728	2.105	1.134	1.297	2.439	1.197
Fluid volumetric rate	V	m^3.s^{-1}	0.0167	0.0136	0.0165	0.0089	0.0102	0.0192	0.0094
Fluid mass rate	M	kg.s^{-1}	58.4	47.4	57.3	38.3	42.2	81.1	40.1

Table VII

SiMn and HCFeMn SAF tapping flow model results for a slag fraction of 1 and slag height at 0.5 m above the taphole.

Parameter	Symbol	Units	SiMn process			HCFeMn process			
			SiMn A	SiMn B	SiMn C	HCFeMn A	HCFeMn B	HCFeMn C	HCFeMn D
Slag density	ρ_{slag}	kg.m^{-3}	2540	2531	2476	2992	2676	2852	2922
Slag viscosity	μ_{slag}	Pa.s	0.74	0.92	0.74	1.54	1.27	0.64	1.44
Liquid mixture density	ρ_{avg}	kg.m^{-3}	2540	2531	2476	2992	2676	2852	2922
Liquid mixture viscosity	μ_{avg}	Pa.s	0.74	0.92	0.74	1.54	1.27	0.64	1.44
Reynolds nr.	Re		379	245	365	112	140	596	124
Friction factor	f		0.084	0.110	0.086	0.190	0.161	0.064	0.176
Coke bed pressure drop	ΔP_1	Pa	26 668	26 741	26 374	29 093	27 541	27 987	28 741
Taphole pressure drop	ΔP_2	Pa	779	661	759	570	570	986	577
Total pressure drop	ΔP_{tot}	Pa	27 448	27 403	27 133	29 663	28 111	28 973	29 318
Fluid flow velocity	u	m.s^{-1}	1.103	0.890	1.091	0.578	0.664	1.339	0.611
Fluid volumetric rate	V	m^3.s^{-1}	0.0087	0.0070	0.0086	0.0045	0.0052	0.0105	0.0048
Fluid mass rate	M	kg.s^{-1}	22.0	17.7	21.2	13.6	14.0	30.0	14.0

Influence of volume fraction slag:

The sensitivity of total tapping flow rate to the fraction slag tapped has been evaluated for the typical HCFeMn and SiMn slags (Table I), tapped at a slag height of 0.5 m above the taphole and using the rule of mixtures to estimate the mixed flow viscosity. Estimated total tapping flow rates for slag fractions between 0.2 and 1 are illustrated in Fig. 12. For slag fractions below 0.2, all flow rates have been estimated to increase to over 0.1 m^3.s^{-1}, and not shown to show differences at the higher slag fractions. Using the rule of mixtures to estimate the average viscosity resulted in viscosity decreasing with increasing alloy fraction, and therefore tapping rates increasing relative to the values at a slag fraction of 1 (Fig. 12). For slag fractions above 0.5, the total tapping rates were estimated to be mostly within or above the range of typical rates derived from Olsen et al.[1]. At slag fractions below 0.5, the total tapping rates were estimated to be significantly higher, as would be expected for mixtures containing predominantly low-viscosity alloy.
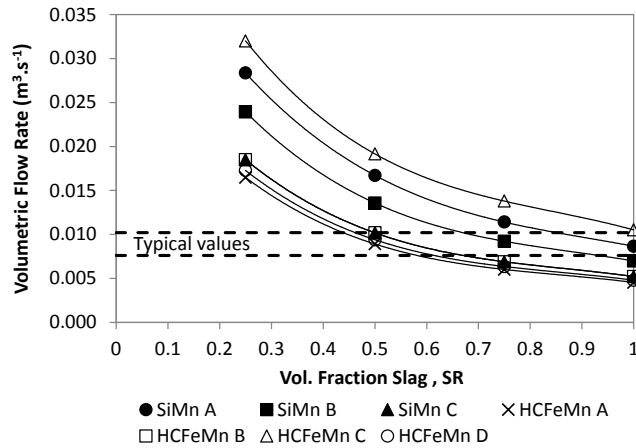
Fig. 12 Total volumetric flow rate as a function of the volumetric slag fraction for typical SiMn and HCFeMn slags, for a slag height of 0.5 m (effective viscosity by the rule of mixtures).

Influence of taphole length and diameter:

The sensitivity of the estimated flow rate to the two taphole dimensions was established separately. The taphole diameter was varied around the baseline value of 0.1 m (for a length of 0.6 m), and the taphole length was then varied around the baseline value of 0.6 m (for a diameter of 0.1 m). As a basis, the slag bath height was set at 0.5 m above the taphole, the alloy height at 0 m, and the volumetric slag fraction at 1, being the case for which the highest flow rates and pressure drops across the taphole were obtained (Table VII). Estimated volumetric flow rates are shown in Fig. 13 as a function of taphole length, and in Fig. 14 as a function of taphole diameter. Results are illustrated with the range of typical flow rates derived from data from Olsen et al.[1] (Table II), which in this case are only the slag rates, since the slag fraction was set at 1. Fig. 13 illustrates small decreases in flow rate of approximately 6% when increasing the taphole length from 0.3 to 3 m. Fig. 14 shows significant increases of flow rate with taphole diameter. A doubling in the taphole diameter from 0.075 to 0.15 m resulted in a doubling of the estimated flow rates. Flow rates can therefore be expected to increase by this amount in relation to wear causing enlargement of the taphole. For the conditions considered here, flow was estimated to remain laminar.
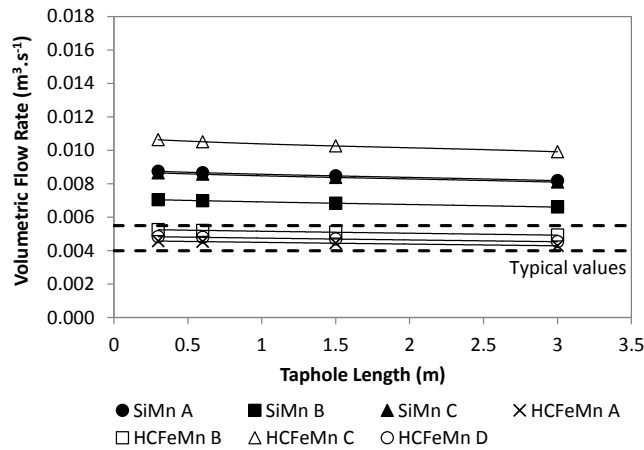
Fig. 13 Total volumetric flow rate as a function of the taphole length for typical SiMn and HCFeMn slags for a slag height 0.5 m and volumetric slag fraction of 1.
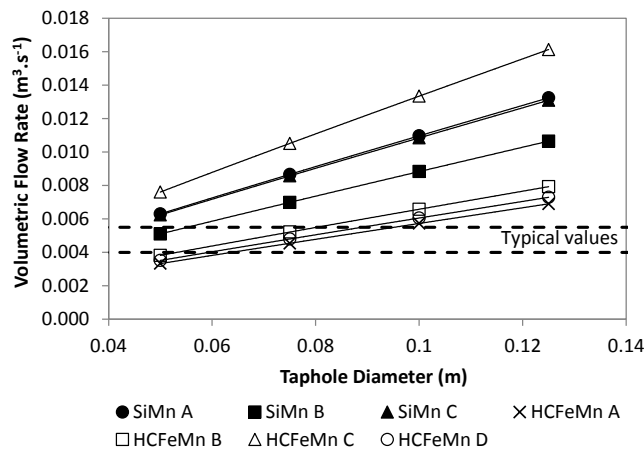

Fig. 14 Total volumetric flow rate as a function the taphole diameter for typical SiMn and HCFeMn slags for a slag height 0.5 m and volumetric slag fraction of 1.

4. CONCLUSIONS

A simplified analytical model is presented to model the tapping flow rate of liquid slag-metal mixtures for HCFeMn and SiMn processes. The model allows for investigating the effect of variations in taphole dimensions and coke bed properties, as well as differences in physicochemical properties caused by fluctuations in chemical composition and temperature during normal operation or due to differences between the HCFeMn and SiMn processes and practices. The model was applied to typical HCFeMn and SiMn process conditions, showing that significant differences can be expected in tapping flow rates from these processes. Generally, SiMn slags were found to have the lowest viscosities, resulting in higher tapping flow rates being calculated. In addition to the slag physicochemical properties, the differences in tapping rates were found also to be strongly dependent on the fraction of slag in the tap stream and properties of the taphole.

The model application results presented suggest that separated flow occurs when tapping a liquid slag-metal mixture under conditions considered. When assuming a finely dispersed liquid mixture, the viscosity was estimated to decrease with an increasing fraction of slag tapped, with calculated flow rates mostly lower than typical values. The simple rule of mixtures approach, associated with separated flow, appeared to provide for a closer approximation of the liquid mixture viscosity as estimated tapping flow rates were mostly within the range of observed values, or higher. Mostly laminar flow was estimated for this model application, with the pressure drop dominant over the coke bed. Turbulent flow was predicted in some cases, for which higher taphole friction factors were calculated. With the focus on tapping a stream of slag only, model results indicated tapping flow rates to be more sensitive to taphole diameter than to taphole length.

It is recommended that this tapping flow model be validated against actual plant measurements for a range of typical slag compositions typical of the HCFeMn and SiMn processes and practices of interest. The model can also be improved by accounting for the variation of slag hydrostatic pressure with height in the inlet pressure boundary condition.

5. TABLE OF SYMBOLS

A: slag viscosity model A-parameter

B: slag viscosity model B-parameter

d: taphole diameter (m)

D: coke bed particle diameter (m)

f: taphole tube friction factor (dimensionless)

f_{app}:   apparent friction factor for developing laminar flow (dimensionless)

$f_{turbulent}$:   apparent friction factor for turbulent flow (dimensionless)

h_{slag}:   slag height (m)

h_{metal}:   metal height (m)

K: viscosity of the dispersed phase divided by the viscosity of the continuous phase (dimensionless)

L: taphole length (m)

M: fluid mass rate (kg.s^{-1})

P_1:   coke bed pressure at taphole inlet (Pa)

P_2:   taphole outer pressure (Pa)

ΔP_1:   coke bed pressure drop (Pa)

ΔP_2:   taphole pressure drop (Pa)

ΔP_{tot}:   total pressure drop over coke bed and taphole ($=\Delta P_1 + \Delta P_2$) (Pa)

r: spherical radius – distance from taphole entrance (m)

Re: Reynolds number (dimensionless)

r_{far}:   far radius of hemisphere (m)

$r_{taphole}$:   taphole radius (m)

SR: slag ratio (vol. fraction slag)

T: temperature (K)

u: average fluid velocity (m.s^{-1})

V: fluid flow volumetric rate (m^3.s^{-1})

$\bar{V}_{298\,K}$:   solid slag partial molar volume at 298 K (m^3.kmol^{-1})

w_{MnO}:   mass fraction MnO in slag (mass fraction)

X: mole fraction of slag component (mole fraction)

X_A: mole fraction amphoterics in slag (mole fraction)

$X_{Al_2O_3}$:   mole fraction Al$_2$O$_3$ in slag (mole fraction)

X_G: mole fraction glass formers in slag (mole fraction)

X_{CaO}: mole fraction CaO in slag (mole fraction)

X_M: mole fraction modifiers in slag (mole fraction)

X_{MgO}: mole fraction MgO in slag (mole fraction)

X_{MnO}: mole fraction MnO in slag (mole fraction)

X_{SiO_2}: mole fraction SiO₂ in slag (mole fraction)

α: ratio parameter in slag viscosity model (dimensionless)

ε: coke bed void fraction (dimensionless)

μ: fluid viscosity (Pa.s)

$\mu_{continuous}$: viscosity of continuous phase (Pa.s)

$\mu_{dispersed}$: viscosity of dispersed phase (Pa.s)

$\mu_{effective}$: effective viscosity (Pa.s)

μ_{liquid}: liquid viscosity (Pa.s)

μ_{metal}: metal viscosity (Pa.s)

$\mu_{mixture}$: liquid slag-metal mixture viscosity (Pa.s)

μ_{slag}: slag viscosity (Pa.s)

μ_r: relative viscosity (Pa.s)

ρ: fluid density (kg.m⁻³)

$\rho_{298\,K}$: solid slag density at 298 K (kg.m⁻³)

$\rho_{1673\,K}$: liquid slag density at 1673 K(kg.m⁻³)

ρ_{liquid}: liquid slag density (kg.m⁻³)

$\rho_{mixture}$: liquid slag-metal mixture density (kg.m⁻³)

ρ_{metal}: metal density (kg.m⁻³)

ρ_{slag}: slag density (kg.m⁻³)

$\rho_{slag\ mixture}$: multiphase slag density (kg.m⁻³)

ρ_{solid}: solid slag density (kg.m⁻³)

$\varphi_{dispersed}$: volume fraction of the dispersed phase (vol. fraction)

φ_m: model fitting parameter with a value of 0.637 used (vol. fraction)

φ_{metal}: volume fraction metal (vol. fraction)

φ_{slag}: volume fraction slag (vol. fraction)

φ_{solids}: volume fraction slag solids (vol. fraction)

ζ: apparent friction factor parameter ($= L/d\ Re$)

6. REFERENCES

1. S.E. Olsen, M. Tangstad and T. Lindstad: *Production of Manganese Ferroalloys*, Tapir Academic Press, Trondheim, 2007.

2. K. Nishioka, T. Maeda, and M. Shimizu: *ISIJ Int.*, 2005, vol. 45, no. 5, pp. 669-676.

3. B. Desai and S. Lenka: *Ironmaking Steelmaking*, 2007, vol. 34, no. 3, pp. 269-271.

4. C. Leu: *Computation Fluid Dynamic Simulation of Blast Furnace Hearth Drainage*, M.S. Thesis, Purdue University, 2010.

5. I. Shao: *Model-based Estimation of Liquid Flows in the Blast Furnace Hearth and Taphole*, D.Tech Thesis, Åbo Akademi University, 2013.

6. M. Kadkhodabeigi, H. Tveit and S.T. Johansen: *ISIJ Int.*, 2010, vol. 51, no. 2, pp. 193-202.

7. M. Iida, K. Ogura and T. Hakone: *ISIJ Int.*, 2008, vol. 48, no. 3, pp. 412-419.

8. *Slag Atlas*, 2nd ed., Verlag Stahleisen GmbH, Dusseldorf, 1995.

9. C.W. Bale, E. Bélisle, P. Chartrand, S.A. Decterov, G. Eriksson, K. Hack, I.H. Jung, Y.B. Kang, J. Melançon, A.D. Pelton, C. Robelin and S. Petersen: *Calphad*, 2009, vol. 33, no. 2, pp. 295–311.

10. K.C. Mills, I. Yuan and R.T. Jones: *J. S. Afr. Inst. Min. Metall.*, 2011, vol. 111, pp. 649–658.

11. R. Roscoe: Br. *J. Appl. Phys.*, 1952, vol. 3, pp. 267–269.

12. K.C. Mills, B.J. Keene: *Int. Mater. Rev.*, 1987, 32, pp. 1-23.

13. R. Pal: *J. Rheol.*, 2001, vol. 45, no. 2, pp. 509-520.

14. J.H. Lienhard IV and J.H. Lienhard V: *A Heat Transfer Textbook*, 3rd ed., Phlogiston Press, Cambridge, MA, 2006.

15. A.J. Ghajar and K.F. Madon: *Exp. Therm Fluid Sci.*, 1992, vol. 5, pp. 129-135.

16. R.B. Bird, W.E. Stewart and E.N. Lightfoot: *Transport Phenomena*, 2nd ed., John Wiley & Sons, Inc., 2007, pp. 182.

17. H. Mølnås: *Compatibility Study of Carbon-based Refractory Utilised in Silicomanganese Production Furnaces*, M.S. Thesis, NTNU, 2011.

18. M. Kadkhodabeigi: *Modeling of Tapping Processes in Submerged Arc Furnaces*, Ph.D Thesis, NTNU, 2011.

19. A.F. Crawley: *Int. Metal. Rev.*, 1974, vol. 19, no. 1, pp. 32-48.

20. I. Jimbo, and A.W. Cramb: *Metall. Trans. B*, 1993, vol. 24, no. 1, pp. 5-10.

21. P.M. Nasch and S.G. Steinemann: *Phys. Chem. Liq.*, 1995, vol. 29, no. 1, pp. 43-58.